Published in final edited form as:
Nat Neurosci. 2019 June 05; 22(7): 1046–1052. doi:10.1038/s41593-019-0418-z.

Central nervous system regeneration is driven by microglia necroptosis and repopulation

Amy F. Lloyd[1], **Claire L. Davies**[1], **Rebecca K. Holloway**[1], **Yasmine Labrak**[2], **Graeme Ireland**[1], **Dario Carradori**[2], **Alessandra Dillenburg**[1], **Eva Borger**[3], **Daniel Soong**[1], **Jill C. Richardson**[4,ϕ], **Tanja Kuhlmann**[5], **Anna Williams**[3], **Jeffrey W. Pollard**[1], **Anne des Rieux**[2], **Josef Priller**[6,7], and **Veronique E. Miron**[1,*]

[1]Medical Research Council Centre for Reproductive Health, The Queen's Medical Research Institute, The University of Edinburgh, Edinburgh, Scotland, United Kingdom

[2]Louvain Drug Research Institute, Advanced Drug Delivery and Biomaterials, Université Catholique de Louvain, Brussels, Belgium

[3]Medical Research Council Centre for Regenerative Medicine, The University of Edinburgh, Edinburgh, Scotland, United Kingdom

[4]Neurosciences Therapeutic Area Unit, GlaxoSmithKline R&D Ltd, Stevenage, England, United Kingdom

[5]Institute of Neuropathology, University Hospital Muenster, Muenster, Germany

[*]**Correspondence to:** Veronique E. Miron, vmiron@ed.ac.uk.
[ϕ]**Present address:** Discovery Research MRL UK, Merck Sharp & Dohme, The London Bioscience Innovation Centre, London, England, United Kingdom.

Data availability statement

The data that support the findings of this study are available from the corresponding author upon request. The RNA sequencing data discussed in this publication have been deposited in NCBI's Gene Expression Omnibus and are accessible through the series GSE118450, accession numbers are GSM3330371 (3 dpl microglia sample 1), GSM3330372 (3 dpl microglia sample 2), GSM3330373 (3 dpl microglia sample 3), GSM3330374 (10 dpl microglia sample 4), GSM3330375 (10 dpl microglia sample 5), GSM3330376 (10 dpl microglia sample 6) (https://www.ncbi.nlm.nih.gov/geo/query/acc.cgi?acc=GSE118450). Raw data (FPKM) is shown in Figure 1D, Figure 1F, and supplementary Figures 1B, 1D, 1E, 1G, 1H, 1K, 1M, 10A, 10B. Processed data is shown in Figure 1, Supplementary Figures 1 and 2, and Supplementary Tables 1-3.

Accession codes

The RNA sequencing data discussed in this publication have been deposited in NCBI's Gene Expression Omnibus and are accessible through GEO series GSE118450, accession numbers are GSM3330371 (3 dpl microglia sample 1), GSM3330372 (3 dpl microglia sample 2), GSM3330373 (3 dpl microglia sample 3), GSM3330374 (10 dpl microglia sample 4), GSM3330375 (10 dpl microglia sample 5), GSM3330376 (10 dpl microglia sample 6) (https://www.ncbi.nlm.nih.gov/geo/query/acc.cgi?acc=GSE118450).

Author contributions:

A.F.L. co-designed the study, carried out the experiments, analysed and interpreted the data, and wrote the manuscript; C.L.D. carried out lesioning experiments, optimized lesion isolation protocols, assisted with flow cytometry, and performed experiments and analysis for RNA sequencing; R.K.H. assisted in lesioning experiments and optimized human tissue staining and analysis protocols; Y.L., D.C., and A.d.R. developed and tested LNCs for microglia targeting; G.I. assisted with genotyping; A.D and D.S. developed remyelination index quantification protocols; E.B. and A.W. provided corpus callosum lesion tissue; J.C.R. provided guidance for experimental design; A.W. and J.W.P. co-supervised the project, assisted with experimental design and interpretation, and manuscript editing; T.K. provided cuprizone tissue and edited the manuscript; A.W. provided human tissue neuropathological mapping; J.P. assisted in experimental design, data interpretation, and manuscript editing; V.E.M. co-designed the study, supervised the project, and guided experimental design, data interpretation, and manuscript preparation.

Competing interests:

A.F.L.'s salary and experiments for this study were co-funded by GlaxoSmithKline. J.C.R. was a full time employee at GlaxoSmithKline at the time of the study.

Europe PMC Funders Author Manuscripts

[6]Department of Neuropsychiatry and Laboratory of Molecular Psychiatry, Charité Universitätsmedizin Berlin, Berlin, Germany

[7]United Kingdom Dementia Research Institute, The University of Edinburgh, Edinburgh, Scotland, United Kingdom

Abstract

Failed regeneration of central nervous system myelin contributes to clinical decline in neuroinflammatory and neurodegenerative diseases, for which there is an unmet therapeutic need. Here, we reveal that efficient remyelination requires death of pro-inflammatory microglia followed by repopulation to a pro-regenerative state. We propose that impaired microglia death and/or repopulation may underpin dysregulated microglia activation in neurological diseases, and reveal novel therapeutic targets to promote white matter regeneration.

Central nervous system (CNS) remyelination reinstates axon health/ function1, yet fails in prevalent neurodegenerative disorders contributing to axon dysfunction/loss for which there is an unmet therapeutic need. These disorders (e.g. multiple sclerosis, ALS, spinal cord injury) are associated with chronic activation of resident immune cells, microglia2–4. Resolution of pro-inflammatory microglia activation (iNOS+ TNFα+ CCL2+) via a transition to a pro-regenerative microglia state (Arg-1+ CD206+ IGF-1+) initiates remyelination3. Remyelination is impaired when this transition is prevented (by depletion of pro-regenerative microglia), or when it fails, identified by prolonged pro-inflammatory microglia presence in aged mice and chronic human brain lesions3. However, the mechanisms underpinning this transition in microglia activation remain unknown.

To reveal these mechanisms, we performed RNA sequencing of microglia isolated from focal demyelinated lesions of young adult mouse corpus callosum induced with the myelin toxin lysophosphatidyl choline (LPC), where regeneration occurs without concomitant damage and timing of microglia activation is defined (Fig. 1A)3. At peak pro-inflammatory (3 dpl) and pro-regenerative microglia activation (10 dpl), microglia were FACS-isolated based on expression of CD11b, lack of expression of neutrophil/ T-lymphocyte markers (Ly6G, CD3), and low expression of CD45 (gating strategy in Supplementary Fig.1A). Cells expressed microglia signature genes post-demyelination (Supplementary Fig.1B); we assessed regulation of two of these genes (*P2ry12*, *Csf1r*) after demyelination versus non-lesion microglia, and observed no significant change at 3 dpl yet upregulation at 10 dpl (Supplementary Fig.1C). Cells did not express markers for border-associated macrophages or monocyte-derived cells (Supplementary Fig.1D). Of the 5000 most highly expressed genes (including non-differentially expressed genes), 57.2% were shared and 21.4% were specific to each time point (Fig. 1B). Microglia expressed genes associated with microglia during developmental myelination5, 6 or neurodegeneration7,8 (Supplementary Fig. 1E-I), some of which were significantly enriched at 10 dpl. 1020 genes were significantly differentially expressed between 3 and 10 dpl ($p<0.05$) (Fig. 1C; Log_2 fold change in Supplementary Table 1), including genes involved in survival/ proliferation (*Birc5*, *Smad2*, *Ccnb1*), anti-oxidant responses (*Keap1*), inflammation (*Tnfrsf1b*, *Jak2*, *Nfkbid*, *Cryba1*, *Gpmnb*, *Socs1*, *Cd40*), remyelination (*Axl*, *Osm*, *Adam8*), and associated with microglia in

neurodegeneration (*Msr1*, *Hdac5*, *Syp*) (Supplementary Fig. 1J). Pathway analysis identified enrichment of chronic inflammation at 3 dpl, and anti-inflammatory responses/ transcriptional regulators at 10 dpl (Supplementary Fig. 2, Supplementary Table 2; Supplementary Fig. 1K). Significantly upregulated genes at 10 dpl included those encoding proteins associated with remyelination/ regeneration (*Matn2*, *Osm*, *Fgf1*, *Cd300lf*), myelination (*Bmp1*, *Cd69*, *Fabp5*), and oligodendrocyte lineage responses [iron export (*Cp*), Wnt pathway inhibition (*Nit1*)] (Fig.1D, Supplementary Fig. 1L). Microglia at both time points showed engagement of phagocytic pathways, by KEGG analysis (‘*fat digestion’* at 3 dpl; ‘*endocytosis’* at 10 dpl; Fig. 1E), Gene Ontology enrichment (e.g. *‘degradation of lipoproteins’* at 3dpl; *‘structural constituent of myelin sheath’* at 10 dpl; Supplementary Fig. 2), and receptor expression (Fig.1F), suggesting engulfment/breakdown of myelin debris throughout remyelination.

Cell death-associated pathways were enriched in microglia at 3 dpl, with i) engagement of KEGG pathways (*‘axon guidance’*, *‘colorectal cancer’*) associated with genes regulating cell death (*Birc5*, *Smad2*, *Ephrb1/2*) (Fig. 1E), ii) ‘*Cell death & Survival*’ identified as a major molecular and cellular function (Fig. 1G) due to regulation of genes associated with death (e.g. TNF receptor signalling, TRAIL, p53; Supplementary Table 3), and iii) most transcriptional regulators upregulated at 3 dpl known to control cell death (Supplementary Table 2; Supplementary Fig. 1M). To determine whether microglia undergo death after demyelination, we analysed IBA-1+ cells in lesions, which were homogenous at 3 dpl, sparse at 7 dpl, and clustered at 10 dpl (Fig. 1I), and decreased in density at 7 dpl (Fig.1H, I). Flow cytometric analysis of microglia ($CD11b^{+}CD45^{lo}$) revealed an increase in death (Annexin-V+ 7-AAD+) at 7 dpl (Fig. 1J, K; gating strategy Supplementary Fig. 3A; Supplementary Fig. 3C). Microglia isolated from sham-lesioned mice at 7 days post-surgery were negative for Annexin-V and 7-AAD (Supplementary Fig. 3B), excluding that death occurred from injection/ cell isolation. Thus, after demyelination and prior to onset of remyelination, microglia die during the transition from pro-inflammatory to pro-regenerative activation.

To investigate mechanisms regulating microglia death after demyelination, we first used *ex vivo* mouse organotypic cerebellar explants which mimic *in vivo* tissue microenvironments and remyelination (Supplementary Fig. 4A). Microglia (CD68+, PU.1+, IBA-1+) in LPC-demyelinated explants were decreased by 1 dpl, intermediate to peaks of pro-inflammatory microglia (iNOS+ CD68+; 0.5 dpl) and pro-regenerative microglia (Arg-1+ CD68+; 7 dpl) (Supplementary Fig. 4B-F). Vehicle (PBS)-treated explants showed no demyelination nor iNOS+ CD68+ cells, with MBP immunoreactivity comparable to fully myelinated untreated slices (Supplementary Fig. 4G-I). Live incorporation of a marker of compromised membrane integrity (propidium iodide; PI) confirmed microglia death prior to cell loss (18-24 hours post-LPC (hpl)) and PI was present in most PU.1+ microglia nuclei by 24 hpl (Supplementary Fig. 4J-M). LPC did not have toxic effects on microglia as no cell loss occurred when primary microglia were treated overnight (Supplementary Fig. 5A). Live imaging of explants from microglia reporter mice (*Csf1r*-eGFP) showed microglia rounding up and rupturing post-LPC, which was not observed in control (Supplementary Videos S1, S2). Microglia were negative for apoptotic markers (cleaved caspase-3, TUNEL), and constitutively positive for pyroptosis marker cleaved caspase-1 even without demyelination

(Supplementary Fig. 5B, C). We then investigated necroptosis, a programmed necrosis whereby a necroptosome complex composed of RIPK1, RIPK3, and MLKL compromises membrane integrity. Necroptosis markers were expressed in IBA-1+ or CD68+ cells after demyelination prior to death: at 3 dpl *in vivo* (Fig. 2A-C; Supplementary Fig.5D; IBA-1 and MLKL co-localization: 34.2 % at 3 dpl vs 7.0 % at 7 dpl) and 12 hpl in explants (Fig. 2D, E). CD68+ cells in sham-injected mice were RIPK3-negative (Fig. 2A). Several genes regulating necroptosis were enriched in the '*Cell death & Survival*' IPA pathways (e.g. *Tnfsf10*, *Bcl3*, *Tnfrsf1b*) (Supplementary Table 3). Lineage tracing of infiltrating monocytes via *Ccr2*-driven RFP expression confirmed that the majority of RIPK3+ cells in lesions *in vivo* were RFP- rather than monocyte-derived (RFP+), and CD68 strongly co-localized with microglial marker Tmem119 (Supplementary Fig.6). We confirmed that microglia necroptosis is a common feature of remyelination by analysing 2 additional *in vivo* demyelination models. In the cuprizone toxin-diet model, RIPK3+ and MLKL+ microglia were significantly increased at remyelination onset and decreased when complete (Supplementary Fig. 7A-D). Mining of published microglia transcriptomes from a model of chronic myelin injury to the spinal cord (MOG-induced experimental autoimmune encephalomyelitis])9 indicated expression of *Ripk3* and *Mlkl* at late stages of disease when remyelination occurs10 (Supplementary Fig. 7E). Therefore, microglia necroptosis is associated with remyelination, regardless of CNS region or mode of injury.

To determine the role of microglia necroptosis in remyelination, we used necrostatin-1, a small molecule which prevents necroptosome activity. At 1 dpl, necrostatin-1 treatment of demyelinated explants prevented loss of CD68+ microglia (Fig. 2F) and maintained iNOS+ CD68+ microglia (Fig. 2G-H), even at 7 dpl when the transition to the pro-regenerative phenotype would normally have taken place (Fig. 2G, H). We observed a decrease in iNOS+ CD68+ cell numbers by 14 dpl (Fig. 2G) indicating either delayed change in activation or apoptosis due to prolonged necroptosis inhibition. Necrostatin-1 significantly hindered remyelination at 7 and 14 dpl compared to vehicle control (Fig. 2I, J). This did not result from directly inhibiting oligodendrocyte or neuronal necroptosis11,12, as only ~3% of oligodendrocyte lineage cells (Olig2+) or neurons (NeuN+) were RIPK3+ post-LPC in explants (Supplementary Fig. 8A-D). Necrostatin-1 treatment of undemyelinated explants had no consequence on MBP immunoreactivity or iNOS expression in CD68+ microglia (Supplementary Fig.8E, F). To determine whether microglia necroptosis is required for remyelination *in vivo*, we aimed to target necrostatin to macrophages by encapsulation in lipidic nanocapsules (LNCs), predicted to be preferentially taken up by phagocytes as shown with other lipid-rich nanoparticle formulations (Fig.2K). Uptake specificity in lesions was verified by injection of DiD-labelled LNCs, with >90% of DiD clusters co-localized with IBA-1+ cells (Fig.2L, N), significantly more than those co-localized with other phagocytic cells [3.9% in astrocytes (GFAP+; Fig. 2L, N) and 1.3% in oligodendrocyte lineage cells (CC1+, Olig1+; Fig.2N, Supplementary Fig. 8G, H)]. 3D reconstruction confirmed internalization of DiD-LNCs within IBA-1+ cells (Fig. 2M; Supplementary Fig.8H). At 3 dpl, necrostatin-loaded LNCs inhibited microglia necroptosis as indicated by decreased MLKL in IBA-1+ cells compared to vehicle (DMSO)-LNCs (Fig. 2O), reducing co-localization of MLKL and IBA-1 from 45.11% to 20.93%. Necrostatin-LNCs did not affect percentage of RIPK3+ CD68+ cells (Supplementary Fig. 8I), as expected given that

necrostatin does not prevent RIPK3 expression but acts downstream to inhibit MLKL recruitment/ activation. Necrostatin-LNCs caused a relative increase in Tmem119+ cells compared to vehicle-LNCs, associated with increased percentage of CD68+ cells expressing iNOS and decreased percentage of those expressing Arg-1 (Fig. 2P). Increased microglia numbers were not due to proliferation, as Ki67+ PU.1+ cell number was significantly downregulated at 3 dpl in Necrostatin-LNC-treated lesions relative to vehicle-LNC control, then negligible by 10 dpl (Supplementary Fig. 8J). Remyelination was impaired at 10 dpl following necrostatin-LNC treatment as indicated by reduced expression of early remyelination marker myelin associated glycoprotein (MAG) (Fig.2Q, R). This was not due to accumulation of myelin debris (identified using MBP which is not yet expressed at this early stage of remyelination) which was equally cleared in both conditions (Supplementary Fig. 8K), consistent with RNA sequencing data suggesting phagocytic capacity of pro-inflammatory microglia (Fig.1E, F; Supplementary Fig.2). Altogether, this data demonstrates the requirement for microglia necroptosis for remyelination to occur, although we acknowledge the possibility that inhibiting necroptosis of a small percentage of other cell types may have also affected remyelination.

We next determined how microglia repopulate to the pro-regenerative phenotype following demyelination. We assessed Nestin expression, which identifies repopulating microglia following experimental depletion13–15. *In vivo* lesions showed increased co-localization of IBA-1 with Nestin from 3 dpl to 7 dpl, which was reduced by 10 dpl when the transition in microglia activation has taken place (Fig. 3A-C). Little to no Nestin was co-localized with IBA-1 in sham control, indicating expression by microglia largely during remyelination (Fig. 3A). Microglia repopulation following experimental depletion has been proposed to occur via: i) *de novo* differentiation of CNS-resident Nestin+ cells14, or ii) proliferation of residual microglia which did not die13, 15. However, these studies examined microglia repopulation in healthy grey matter, where the microenvironment may differ from injured white matter. To investigate microglia repopulation following demyelination, we induced focal lesions in mice in which Nestin promoter-driven tdTomato (tdT) expression is inducible (*Nes*-CreERT2;RCL-tdT), allowing labelling of Nestin+ cells prior to demyelination. Of all tdT+ cells, the proportion which were $CD11b^{+}$ $CD45^{lo}$ (gating Supplementary Fig. 9A) increased from 3 dpl to 7 and 10 dpl (Fig. 3D, E; Supplementary Fig. 9B). Although the proportion of all $CD11b^{+}$ $CD45^{lo}$cells which were tdT+ increased at 7 dpl versus 3 dpl and sham control, these only represented <5% of total microglia (Fig. 3F, G) suggesting that repopulation *in vivo* is mediated primarily by residual microglia.

Microglia repopulation also occurred in the explant model (Supplementary Fig.4C). Recombination in Nestin+ cells prior to LPC lead to detection of some tdT+ IBA-1+ cells only during early repopulation (1-2 dpl), which were undetectable by 7 dpl (Supplementary Fig. 9C-F); tdT+ cells expressed neural stem cell markers Musashi-1 and Sox2, but not GFAP (Supplementary Fig.9G). We assessed the contribution of residual microglia to repopulation in explants derived from *Cx3cr1*-CreER; RCL-tdT mice (Supplementary Fig. 9H) in which tdT labelled IBA-1+ microglia (Supplementary Fig. 9I) but not the oligodendrocyte lineage, previously suggested to express CX3CR1 (Supplementary Fig. 9J). The majority of repopulated IBA-1+ cells were tdT+ and therefore derived from residual microglia (Supplementary Fig.9K-M), with 30% being Nestin+ at 2dpl (Supplementary Fig.

9N, O). Therefore, lineage tracing supports that microglia repopulation during remyelination occurs primarily from residual microglia.

To investigate necroptosis and repopulation in human white matter disease, we examined multiple sclerosis (MS) lesion subtypes: i) active lesions, which have high densities of macrophages, positively correlated with remyelination and oligodendrocyte precursor abundance, ii) chronic inactive lesions, which have low potential for remyelination, and iii) fully remyelinated lesions (Supplementary Table 4). Although densities of CD68+ cells undergoing necroptosis (RIPK3+ and MLKL+; Fig. 3H, I, K) or PU.1+ cells undergoing repopulation (Nestin+; Fig. 3J, L) were present in all MS lesion types, these were only significantly increased in active lesions compared to control. This may suggest abundance of cues for pro-remyelination microglial responses in an inflammatory environment.

We next investigated molecular pathways controlling microglia during remyelination. IPA analysis indicated regulation of Type-1 interferon (IFN) signalling, with '*Interferon signalling*' and '*Role of JAK1, JAK2, and TYK2 signalling in Interferon signalling*' identified as top canonical pathways, and top predicted upstream regulators included IFNα/β, IFNAR, STAT1, IRF7, and IRF3 (P=0.00013, 0.00089, 0.000045, 0.0071, 0.000086, respectively). Microglia expressed genes encoding the IFNα/β receptor (*Ifnar1*, *Ifnar2*) and IFN-associated genes linked with microglia during remyelination16 (Supplementary Fig. 10A, B), and CD68+ cells expressed IFNα/β receptor subunit 2 (IFNAR2) protein *in vivo* (Fig. 3M). IFN signalling, assessed by nuclear phospho-STAT1, was only active at 7 dpl *in vivo* and was selective to 58 ± 7% of PU.1+ nuclei (Fig. 3N,O), consistent with the largest microglia subpopulation in this model having an interferon signature 16. We assessed the role of Type-1 IFN signalling using explants where microglia death and repopulation are temporally separated and can be investigated in isolation. Using a neutralizing antibody against IFNAR2 did not significantly affect PU.1+ microglia numbers at 1 dpl compared to IgG isotype control (Fig. 3P), therefore did not prevent microglia death. A significant increase in PU.1+ cells was observed from 1 dpl to 7 dpl in controls but not following IFNAR2 blockade (Fig. 3P), suggesting impaired microglia repopulation. PU.1+ cells were significantly reduced in anti-IFNAR2 IgG conditions relative to control at 7 dpl (Fig. 3P, Q), associated with decreased phospho-STAT1+ PU.1+ microglia (Supplementary Fig. 10C). Consequently, blocking IFNAR2 impaired early remyelination at 7 dpl relative to control (Fig. 3R, S). Altogether, this data supports a regenerative role for Type-1 IFN signalling in regulating the repopulation of white matter microglia during efficient remyelination.

In summary, our data reveal that remyelination is driven by pro-inflammatory microglia necroptosis and repopulation to a regenerative state. Whereas necroptosis of other cell types 11,12 is associated with demyelination and neurodegeneration, we show a regenerative role for necroptosis in shutting down pro-inflammatory microglial activation to support remyelination. Although previous studies identified the capacity of microglia to repopulate following experimental depletion in healthy13–15, aged17, irradiated18, or neurodegenerating brain19, we show that this feature can also serve to reinstate microglia after naturally occurring death following white matter injury, while regulating microglia activation. We reveal that microglia repopulation during white matter remyelination is positively regulated by Type-1 IFN signalling. This contrasts with its deleterious role in

repopulated microglia selectively in grey matter following experimental depletion20, highlighting CNS region-specific consequences of IFN signalling in microglia. We propose that targeting pro-inflammatory microglia death may represent a novel strategy to dampen chronic CNS white matter inflammation, and support a regenerative response to reinstate myelin integrity.

Methods

Animals

Experiments were performed under a UK Home Office project licence issued under the Animals (Scientific Procedures) Act. Animals were housed at 6 animals per cage in a 12 hour light/dark cycle with unrestricted access to food and water. Wild type CD1 mice were used for organotypic cerebellar explant cultures and C57Bl6/J mice were used for *in vivo* demyelination experiments. To track monocyte infiltration into *in vivo* lesions, we used heterozygous *Ccr2* knock-in reporter mice (B6;129(Cg)-*Ccr2*$^{tm2.1lfc}$/J). For lineage tracing, Ai9 (B6;129S6-Gt(ROSA)26Sor$^{tm9(CAG-tdTomato)Hze}$/J) were crossed with C57Bl6-Tg(*Nes*-CreERT2)KEisc/J to induce tdTomato expression in Nestin+ cells, or crossed to *Cx3cr1*-CreER to induce tdTomato expression in microglia. Recombination *in vivo* was induced by 2 subcutaneous injections of tamoxifen (2 mg in 200 μl of corn oil; Sigma-Aldrich T5648) 48 hours apart, 5-7 days prior to brain lesioning. Recombination in explants was induced by overnight treatment with 1 μM 4-hydroxy-tamoxifen (4OHT; Sigma-Aldrich), followed by three washes and an additional 3 media changes over the course of the subsequent week, prior to demyelination. For live imaging, MacGreen mice (B6N.Cg-Tg(Csf1r-EGFP)1Hume/J) were used. Sprague-Dawley rats were used for primary microglial cultures. All animals were purchased from Jackson Laboratories.

Organotypic Cerebellar Explant Cultures

Cerebellum and hindbrain were isolated from P0–P2 CD1 mouse pups of both sexes and sectioned sagittally at 300 μm on a McIlwain tissue chopper. Explants were plated onto Millipore-Millicell-CM mesh inserts (Fisher Scientific) in 6-well culture plates at 6 explants per insert for immunofluorescence or 3 explants per insert for live imaging. Explant culture media consisted of 50% minimal essential media, 25% heat-inactivated horse serum, 25% Earle's balanced salt solution (all from GIBCO), 6.5 mgml^{-1} glucose (Sigma-Aldrich), 1% penicillin-streptomycin (Life Technologies), 1% Glutamax (Life Technologies) and 1% HEPES (Invitrogen), and was changed every 2–3 days. Demyelination was induced at 21 days *in vitro* by application of 0.5 mg.ml^{-1} lysophosphatidyl choline (LPC; Sigma Aldrich) for 18-20 hours which was subsequently washed off in fresh media for 10 minutes; comparisons were made to vehicle (phosphate buffered saline; PBS)-treated explants. Necrostatin-1 (10 μM; Sigma-Aldrich) or vehicle (DMSO; 1:1000) was supplemented to media upon LPC treatment and in each subsequent media change prior to fixation. Propidium iodide (25 μg.ml^{-1}; Sigma-Aldrich) was supplemented to the media for the last 1 hour prior to fixation, and explants were washed thrice in PBS before fixation in the dark. Explants were fixed in 4% PFA for 10 minutes. Each n is the average of 3 explants from 1 litter, with 3 – 5 litters per time point/ condition. Neutralizing antibody against IFNAR2

(R&D Systems, AF1083; 5 μg/ml final concentration), or goat isotype IgG control of matched concentration, was applied to explants up to 1 and 7 days post-LPC.

Immunofluorescent staining of explant cultures

Explants were permeabilized and blocked for 1 hour in 5% horse serum and 0.3% Triton-X 100 in PBS, and primary antibodies were applied for 2 nights overnight at 4°C in a humid chamber. Primary antibodies used include rat anti-CD68 (Abcam, ab53444, 1: 100), rabbit anti-IBA-1 (Wako Chemicals, 019-19741, 1:50), goat anti-PU.1 (Santa Cruz Biotechnology, sc5949, 1:100), mouse anti-iNOS (BD Biosciences, 610329, 1:100), goat anti-Arginase-1 (Santa Cruz Biotechnology, sc18355, 1:50), rabbit anti-RIPK3 (Novus Biologicals, NBP1-77299, 1:100), rat anti-MLKL (Merck-Millipore, MABC604, 1:100), rabbit anti-cleaved Caspase-3 (BD Pharmingen, 559565, 1:100), mouse anti-cleaved Caspase-1 (Santa Cruz Biotechnology, sc22165, 1:100), rat anti-myelin basic protein (MBP; AbD Serotec, MCA409S, 1:250), chicken anti-neurofilament heavy chain (NF-H; Encor Biotechnology, CPCA-NF-H, 1:10,000), mouse anti-Nestin (Abcam, ab6142, 1:100), rabbit anti-Olig2 (Merck, AB9610, 1:100), rabbit anti-GFAP (DAKO, Z0334, 1:500), mouse anti-NeuN (Merck Millipore, MAB377, 1:100), rabbit anti-Musashi-1 (Abcam, ab52865, 1:100), mouse anti-Sox2 (Abcam, ab171380, 1:100), mouse anti-phospho-STAT1 (P-Y701) (Abcam, ab29045, 1:100). Subsequent to washes in PBS, fluorescently conjugated secondary antibodies were applied for 2 h at 20–25°C in a humid chamber (anti-goat IgG (A21432, A11055), anti-rabbit IgG (A11034, A21206, A10042, A11011), anti-rat IgG (A21434, A11006, A21247), anti-mouse IgG (A31570, A21235, A31571, A21042), and anti-chicken IgG (A11039)) (1:1000, Invitrogen). Explants were counterstained with Hoechst, mounted on slides and coverslipped with Fluoromount-G (Southern Biotech). Z-stacks of explants were acquired with an Olympus spinning disk confocal microscope using a 20X objective with Slidebook 6 software. Remyelination in explants was assessed by determining area of co-localization of MBP and NF-H signal normalized to NF-H pixel counts using Volocity 6.3 software (Perkin Elmer).

Live imaging of explant cultures

An insert with cultured explants was adhered by the feet to a single 4 cm petri dish with molten wax and left briefly to dry. Media was first pipetted into the petri dish to diffuse under the mesh then gently pipetted onto the surface of mesh. Z-stacks were acquired using a 20X wet-immersion objective on the Olympus spinning disk confocal microscope using Slidebook 6 software, incubated at 37°C (high humidity) and 5% CO_2. Large Z-stacks were acquired to ensure the explant was always in focus, and maximum projection videos are shown.

Focal demyelinating lesion induction

10 week-old male C57Bl/6J mice were anaesthetized with isoflurane before being stereotaxically injected with 2 μl of 1% lysolecithin (LPC; vol/vol) into the corpus callosum. Control mice underwent the same procedure with a sham injection. Mice were allowed to recover before sacrifice by perfusion-fixation at 3, 7, and 10 days post LPC (dpl) with 4% paraformaldehyde (PFA) for immunofluorescence, or 3.8% sodium citrate in phosphate buffered saline (PBS) for flow cytometric analysis. The former were post-fixed overnight

with 4% PFA, cryoprotected in sucrose, and cryosectioned at 12 μm thickness. A minimum of 3 animals were analyzed per time point.

Lipidic nanocapsule (LNC) formulation

Kolliphor HS15® (0.169 g), Lipoïd® (0.15 g; Lipoid Gmbh), NaCl (0.0178 g), Labrafac® (0.2056 g; Gattefosse SA) and water (0.592 g) were mixed under gentle magnetic stirring at 50°C for 5 min. The solution was progressively heated (90°C) and cooled (60°C) three times. During the last cooling, cold water (2.408 g at 4°C) was added at 72-74°C under high-speed stirring. Necrostatin-1-loaded LNCs were prepared by adding 25.9 μl of necrostatin-1 stock solution (30 mg/ml in DMSO) during the last cooling of LNC preparation. Control LNCs were prepared following the same protocol using DMSO. Fluorescent LNCs (1,1'-Dioctadecyl-3,3,3',3' Tetramethylindodicarbocyanine, 4-Chlorobenzenesulfonate Salt; DiD; ThermoFisher Scientific) were prepared with the same protocol using 220 μl of DiD solution (1 mg/ml in absolute ethanol). The nanoparticles were filtered on a sterile 0.2 μm filter and stored at 4°C until further use. The concentration of necrostatin-loaded LNC stock solution was 1 mM of necrostatin-1 and 126 mg/ml of nanoparticles. Size, ζ-potential and PDI of nanoparticles were measured using a Malvern Zetasizer Nano ZS (Malvern Instruments) (N=3, n=3). For the measurement of size and PDI, samples were diluted 1/100 (v/v) in water. For the measurement of ζ-potential, samples were diluted 1/100 (v/v) in NaCl 10 mM. The encapsulation efficiency of necrostatin-1 was calculated by using the following formula:

$$Encapsulation\ Efficiency = \frac{Necrostatin1\ total\ (ug)\ -\ non\ encapsulated\ Necrostatin1\ (ug)}{Necrostatin1\ introduced\ in\ the\ formulation\ (ug)} * 100$$

Necrostatin-1 was extracted from necrostatin-1 LNC by dissolution in methanol at a ratio 1:20 (v/v) (‘Necrostatin-1 total’). Necrostatin-1 was quantified by Reverse phase-High Liquid Chromatography (Waters) with a Macherey-Nagel 125/4 NUCLEODUR 100-5 C 18 column. A gradient mobile phase was composed of 0.1 % TFA in water (A) and 0.1% TFA in acetonitrile (B). The gradient was set as follows: for the first 2 min, the gradient was set at 80% of A and 20% B. Then, A decreased to 60 % for the 3 following minutes and for the last 2 min, A decreased to 20%. The flow was set for both solutions at 1 ml/min with a volume of injection of 20 μl and the detection wavelength was set at 269 nm. To determine the percentage of non-encapsulated necrostatin-1, necrostatin-1 LNCs were centrifuged in a VIVAPSIN 500 with a membrane that possess a 30 KDa MWCO at 13,000 g for 10 min and the filtered solution was collected and quantified by Reverse Phase High Liquid Chromatography. The properties of the LNCs were as follows: i) necrostatin-1 LNCs: 54.2 nm/ 0.05 PDI/ -2.0 mv ζ–potential/ 263.8 μg/ml/ 100% encapsulation efficiency, ii) DMSO LNCs: 56.4 nm/ 0.06 PDI/ -1.7 mv ζ–potential/ 0.86% (vol/vol) concentration, iii) DiD LNCs: 64.1 nm/ 0.08 PDI/ -1.8 mv ζ–potential/ 14.7% (vol/vol) concentration. LNCs were stereotaxically injected into the corpus callosum of adult mice at the time of lesioning, and mice sacrificed at 3 or 10 dpl. 3D surface view in Slidebook 6 was used for 3D rendering to visualize DiD-LNC localization.

Europe PMC Funders Author Manuscripts

Microglia isolation and RNA extraction/ sequencing

Lesioned corpus callosum of 8-12 week old male C57Bl6J mice was homogenized using a 2 ml Dounce and filtrated (250 μm filter; Pierce). Following a spin at 600 g for 5 min (with brake), cells were resuspended in 100 % fetal bovine serum (FBS) and 33 % Percoll (1:10), overlaid with 1 ml of 10 % FBS, and spun for 15 min at 800 g at 4°C without brake. The cell pellet was washed in FACS buffer and spun for 10 min at 600 g at 4°C, and incubated in anti-mouse CD16/32 Fc-block (Clone 93, BioLegend, 1:200) on ice for 10 min. Fluorescently-conjugated antibodies CD11b-PeCy7 (Clone M1/70, Invitrogen, 1:100), CD45-BV605 (Clone 30D11, Biolegend, 1:200), Ly6G-PerCP Cy5 (Clone 1A8, BioLegend, 1:200), and CD3-APC (Clone 17A2, BioLegend, 1:200) were applied on ice for 30 min. Following centrifugation and filtration (30 μm), cells were sorted by flow cytometry into FBS-coated Eppendorf tubes on ice (BD FACSAria Fusion, 100 μm nozzle). Use of differential CD45 expression (on the logarithmic scale) to distinguish between microglia (lo) and infiltrating monocyte-derived macrophages (hi) in white matter injury has been previously validated using transgenic reporters and bone barrow chimeras. Cells were spun at 800 g for 5 min, resuspended in RLT Plus buffer with β-mercaptoethanol, and centrifuged at 10,000 rpm for 2 min in QIAshredder tubes (Qiagen). RNA was extracted using the AllPrep DNA/RNA/miRNA kit (Qiagen) as per the manufacturer's instructions, and quantity/quality analyzed using the Bioanalyser 2100 (Agilent) and RNA 6000 Pico kit (Agilent) as per the manufacturer's instructions. cDNA production/ library preparation was performed using the NuGEN Ovation RNAseq System v2 kit (NuGEN) by BGI (Hong Kong). End Repair Mix was added to the amplified cDNA and incubated at 20°C for 30 min. AxyPrep Mag PCR clean up kit (Axygen) was used to purify the end-repaired DNA, which was then combined with A-tailing Mix (Enzymatic) and incubated at 37°C for 30 min. Adaptors (Invitrogen) were ligated to the Adenylate 3' ends DNA, and incubated at 16°C for 16 h. Insert size was used to select the adaptor-ligated DNA fragments. Several rounds of PCR amplification with PCR Primer cocktail (Invitrogen) and PCR Master Mix (New England Biolabs) were performed to enrich the adaptor-ligated DNA fragments to produce the final library, purified using AxyPrep Mag PCR clean up kit (Axygen). The final library average molecule length was determined using the Bioanalyser 2100 using the DNA 1000 kit (Agilent) and was quantified by real-time qPCR (TaqMan probe). cBot (Illumina) was used to amplify the libraries to generate the cluster on the Flow Cell (HiSeq 4000, Illumina). An average of 40 million clean 100 paired-end reads (read lengths approximately 100 bp) were achieved per sample, with >91% uniquely mapped reads. Data was processed to remove adaptors and low quality reads from raw reads.

Bioinformatics

Raw data analysis was carried out by Fios Genomics Ltd (Edinburgh, United Kingdom). RNAseq data was pre-processed and aligned to the mouse genome (GRCm38) using STAR aligner, and the number of mapped read-pairs per gene were quantified based on the GENCODE vM12 annotation. A total of 6 samples (3 per time point) were QC analyzed using the 'array Quality Metrics' package in Bioconductor. Data were normalized using trimmed mean of M values (TMM) and transformed using VOOM to Log_2-counts per million, with associated precision weights. Comparisons were undertaken using linear modelling using Limma package in Bioconductor to determine differentially expressed

genes ($p<0.05$); empirical Bayesian analysis for Log_2 fold change was applied. Differentially expressed genes were used for functional enrichment analysis by investigation of Kyoto Encyclopaedia of Genes and Genomes (KEGG) pathways ($p<0.05$), Gene Ontology (GO) terms ($p<0.05$), Venny 2.1 (*http://bioinfogp.cnb.csic.es/tools/venny/*), and Ingenuity Pathway Analysis (IPA) ($p<0.05$).

Real-time quantitative Polymerase Chain Reaction

Real-time (RT) quantitative polymerase chain reaction (qPCR) was run using BioRad Custom PrimePCR plates, as per the manufacturer's instructions. Briefly, cDNA was synthesized using 5x iScript Advanced Reaction Mix and iScript Advanced Reverse Transcriptase (BioRad) at 46 °C for 20 min then 95 °C for 1 min. cDNA samples were mixed with 2x iTaq Universal SYBR-green Supermix and iScript Reverse Transcriptase. The RT qPCR was performed at 50 °C for 10 min, 95 °C for 1 min, 95 °C for 15 sec (40 cycles), 60 °C for 60 sec (40 cycles). Data was analyzed using CFX manager and presented as $2^{-\Delta Ct}$.

Immunofluorescent staining of *in vivo* focal lesions

Sections of frozen tissue were air dried for 15 minutes before being permeabilized and blocked for 1 hour (5% horse serum and 0.3% Triton-X-100 in PBS) then incubated with primary antibodies overnight at 4°C in a humid chamber. Primary antibodies used include rabbit anti-Tmem119 (Abcam, ab209064, 1:100), rat anti-CD68 (Abcam, As53444, 1: 100), rabbit anti-IBA-1 (Wako Chemicals, 019-19741, 1:50), rabbit anti-RIPK3 (Novus Biologicals, NBP1-77299, 1:100), rat anti-MLKL (Merck-Millipore, MABC604, 1:100), mouse anti-iNOS (BD Bioscience, 610329, 1:100), goat anti-Arginase-1 (Santa Cruz Biotechnology, sc18355, 1:50), mouse anti-Nestin (Abcam, ab6142, 1:100), mouse anti-MAG (EMD Millipore, MAB1567, 1:100), rat anti-MBP (AbD Serotec, MCA409S, 1:250), rabbit anti-Ki67 (EMD Millipore, AB9260, 1:100), mouse anti-Olig1 (EMD Millipore, MAB5540, 1:100), mouse anti-phospho-STAT1 (P-Y701; Abcam, ab29045, 1:100), rabbit anti-IFNAR2 (Abcam, ab56070, 1:100). Subsequent to washes in PBS, fluorescently conjugated secondary antibodies were applied for 2 h at 20–25°C in a humid chamber (anti-rabbit IgG (A11034, A21206, A10042, A11011) and anti-rat IgG (A21434, A11006, A21247) all at a concentration of 1:1000 (all from Invitrogen). Slides were counterstained with Hoechst and coverslipped with Fluoromount-G (Southern Biotech). Images were acquired with an Olympus spinning disk confocal microscope with a 20X or 60X objectives with Slidebook software. Percentage of IBA-1/ Nestin or Tmem119/ CD68 co-localization was measured by determining area of co-localization relative to total IBA-1 or CD68 pixel counts, respectively, using Volocity 6.3 software (Perkin Elmer). MAG intensity within lesions was quantified using Adobe Photoshop CS4 with respective background intensity outside the lesion subtracted.

Flow Cytometry

Focal demyelinated lesions of the corpus callosum of 8-12 week old C57Bl6J male mice were dissected out and homogenized with a 2 ml dounce. A Percoll (Sigma-Aldrich) gradient was used to isolate cells from myelin debris. Samples were blocked with Fc-block [LEAF-purified anti-mouse CD16/32 (Biolegend, 101321)], then incubated with fluorochrome-conjugated antibodies CD11b-PeCy7 (eBioscience, 25-0112-82, 1:100) and

CD45-BV605 (Biolegend, 103139, 1:100) for 30 minutes on ice, followed by incubation with 'FITC Annexin-V apoptosis detection kit with 7-AAD' for 15 minutes at room temperature (Biolegend, 640922, 1:20). Following washes in buffer, samples were run on the BD LSR Fortessa (6 laser) analyser, and analysed using FlowJo version 9/10 software (FlowJo LLC).

Primary microglia cultures

Microglia were derived from mixed glial cultures of P0-P3 Sprague-Dawley rats of both sexes by differential adhesion, as previously described3. Cells were plated on poly-*D*-lysine-coated 16-well glass chamberslides (Lab-TEK) at 5 x 10^4 cells per well in Dulbecco's Modified Essential Media (DMEM) containing 4.5 g/L glucose, l-glutamine, pyruvate, 10% fetal calf serum (vol/vol) and 1% penicillin/streptomycin (vol/vol). Treatment included lysophosphatidyl choline (0.5 $mg.ml^{-1}$), (Sigma-Aldrich) prior to fixation with 4% paraformaldehyde (Sigma) for 10 min. Cells were blocked for 1 hour and incubated with primary antibodies at room temperature for 1 hour, for 1 hour at room temperature prior to counterstaining with Hoechst, mounting onto slides and coverslipping with Fluoromount-G.

Immunofluorescent staining of cuprizone tissue

Paraffin-embedded sections of tissue from cuprizone-fed mice underwent deparaffinization using Histoclear (2 x 10 min) and a gradient of ethanol (EtOH) concentrations, each for 5 minutes in the following order: 2 x 100%, 1 x 95%, 1 x 70% and 1 x 50%, before being washed in Tris-buffered saline (TBS) for 3 x 5 minute washes. Slides were then placed in Vector Unmasking Solution under high heat and pressure for 20 minutes before a final TBS wash. Slides were permeabilized and blocked for 1 hour (5% horse serum and 0.3% Triton-X-100 in PBS) before incubation with primary antibodies overnight at 4°C in a humid chamber. Microglia/macrophages were detected with rat anti-CD68 (Abcam, Ab53444, 1: 100) and cell death was assessed using rabbit anti-RIPK3 (Novus Biologicals, NBP1-77299, 1:100) and rat anti-MLKL (Merck-Millipore, MABC604, 1:100). Following washes in PBS, fluorescently conjugated secondary antibodies were applied (Invitrogen, 1:1000). Slides were counterstained with Hoechst and coverslipped with Fluoromount-G (Southern Biotech). Images were acquired with an Olympus spinning disk confocal microscope using a 60X objective with Slidebook 6 software. 3 animals were analyzed per time point.

Human Tissue

Post-mortem tissue from multiple sclerosis (MS) patients and controls that died of non-neurological causes were obtained via a UK prospective donor scheme with full ethical approval from the UK Multiple Sclerosis Tissue Bank (MREC/02/2/39) and their use was in accord with the terms of the informed consents. Diagnosis of MS was confirmed by neuropathological means by F. Roncaroli (Imperial College London) and clinical history was provided by R. Nicholas (Imperial College London). Snap frozen unfixed tissue blocks (2 × 2 × 1 cm) were cut at 10 μm and stored at −80°C. Lesions were classified according to the International Classification of Neurological Disease using Luxol Fast Blue staining and CD68+ immunoreactivity. Following washes in 0.1% Tween-20 (vol/vol) in Tris-buffered saline (TBS), sections were microwaved in Vector unmasking solution for 10 minutes, washed once, and endogenous phosphatase and peroxidase activity blocked for 5 minutes

(Bloxall, Vector). Tissue was incubated with primary antibodies in a humid chamber overnight. Sections were then washed in TBS and stains visualized by Vector Blue substrate kit according to the manufacturer's instructions (maximum 15 minutes). For co-staining, sections were washed thrice and re-blocked to quench any remaining phosphatase activity (Bloxall, Vector) prior to application of primary antibody then developed using Vector Red substrate kit according to the manufacturer's instructions (maximum 15 minutes). Following washes in water, the sections were counterstained with Hoechst and coverslipped with Fluoromount-G. Primary antibodies used include goat anti- CD68 (Santa Cruz Biotechnology, sc7082, 1:100), mouse anti-Nestin (Santa Cruz Biotechnology, sc23927, 1:100), goat anti-PU.1 (Santa Cruz Biotechnology, sc5949, 1:100), rat anti-MLKL (Merck-Millipore, MABC604, 1:100) and rat anti-RIPK3 (Novus Biologicals, NBP1-77299, 1:100). Entire tissue sections were imaged using a Zeiss AxioScan Z.1 SlideScanner, and digital lesion maps were prepared for each tissue in Zeiss Zen2 software using Luxol Fast Blue-stained sections. Fields of 360 μm × 360 μm were counted per lesion and counts were multiplied to determine density of immunopositive cells per mm^2. For quantification of Nestin+ PU.1+ cells, staining with blood vessel morphology was excluded from counts.

Statistics

Details on experimental design and reagents can be found in the Life Sciences Reporting Summary. For animal experiments, power was calculated by two-sided 95% confidence interval using the normal approximation method using OpenEpi software and gave between 88-100% power for all experiments. Animals were randomly selected for experimental groups, and littermates were compared for all treatment groups. All manual cell counts for explants cultures, *in vivo* lesioned tissue, and MS tissue were performed in a blinded manner. Data are represented as mean ± s.e.m. from a minimum of 3 mice (*in vivo* experiments) or litters (explants). Data distribution was assessed using the Kolmogorov-Smirnov test. Data was statistically analyzed by 2-tailed Student's *t*-test or Mann-Whitney test for ≤2 comparisons, one sample *t*-test for analysis of normalized data or comparison to sham, and either Kruskal-Wallis test with Dunn's Multiple Comparison post-test or One-way ANOVA with Sidak's post-test (for select comparisons between groups) for ≥3 comparisons. P values of ≤ 0.05 were considered statistically significant at a confidence interval of 95%. Data handling and statistical processing was performed using Microsoft Excel and GraphPad Prism 7 and 8 Software. Diagrams were created with BioRender software.

Supplementary Material

Refer to Web version on PubMed Central for supplementary material.

Acknowledgements

This work was funded by a Biotechnology and Biological Sciences Research Council (BBSRC)-Collaborative Award in Science and Engineering (CASE) studentship in collaboration with GlaxoSmithKline (V.E.M., J.C.R.; BB/M502777/1), a Medical Research Council and United Kingdom Multiple Sclerosis Society Career Development Award (V.E.M.; MR/M020827/1), funds from the Medical Research Council Centre for Reproductive Health (MR/N02256/1) and the Wellcome Trust (J.W.P.; 101067/Z/13/Z), and a Momentum Award from the United Kingdom Dementia Research Institute (J.P.). The cuprizone studies were supported by the German Research Foundation (T.K.; SFB-TR128-B7). The *Cx3cr1*-CreER experiments were supported by the German Research Foundation (J.P.; SFB-TR167). The LNC studies were supported by grants from F.R.S.-FNRS (A.d.R. and Y.L.), the Fondation

Charcot Stichting and the International Foundation for Research in Paraplegia (A.d.R.). We thank the United Kingdom Multiple Sclerosis Society Tissue Bank for providing tissue, F. Roncaroli for neuropathological diagnosis of MS lesions, and R. Nicholas for providing clinical history of MS patients. We also thank I. Molina-Gonzalez, M. Tzioras, N. Fullerton, C. Watkins, C. Böttcher, and J.Jamal El-Din for technical support, and O. Dando for helpful discussions.

References

1. Franklin RJM, Ffrench-Constant C. Nat Rev Neurosci. 2017; 18:753–769. [PubMed: 29142295]
2. Frakes A, et al. Neuron. 2014; 81:1009–1023. [PubMed: 24607225]
3. Miron V, et al. Nature Neuroscience. 2013; 16:1211–1218. [PubMed: 23872599]
4. Kigerl K, et al. J Neurosci. 2009; 29:13435–13444. [PubMed: 19864556]
5. Wlodarczyk A, et al. EMBO J. 2017; 36:3292–3308. [PubMed: 28963396]
6. Hagemeyer N, et al. Acta Neuropathologica. 2017; 134:441–458. [PubMed: 28685323]
7. Keren-Shaul H, et al. Cell. 2017; 169:1276–1290. [PubMed: 28602351]
8. Krasemann S, et al. Immunity. 2017; 47:566–581. [PubMed: 28930663]
9. Lewis N, Hill J, Juchem K, Stefanopoulos D, Modis L. Journal of Neuroimmunology. 2014; 277:26–38. [PubMed: 25270668]
10. Mei F, et al. eLIFE. 2016
11. Ofengeim D, et al. Cell Reports. 2015; 10:1836–1849. [PubMed: 25801023]
12. Cassamo A, et al. Nature Neuroscience. 2017
13. Bruttger J, et al. Immunity. 2015; 43:92–106. [PubMed: 26163371]
14. Elmore M, et al. Neuron. 2014; 82:380–397. [PubMed: 24742461]
15. Huang Y, et al. Nat Neurosci. 2018
16. Hammond TR, et al. Immunity. 2018
17. Elmore MRP, et al. Aging Cell. 2018; 17:e12832. [PubMed: 30276955]
18. Krukowski K, et al. Sci Rep. 2018; 8:7857. [PubMed: 29777152]
19. Rice RA, et al. Glia. 2017; 65:931–944. [PubMed: 28251674]
20. Rubino SJ, et al. Nat Commun. 2018; 9:4578. [PubMed: 30385785]

Europe PMC Funders Author Manuscripts

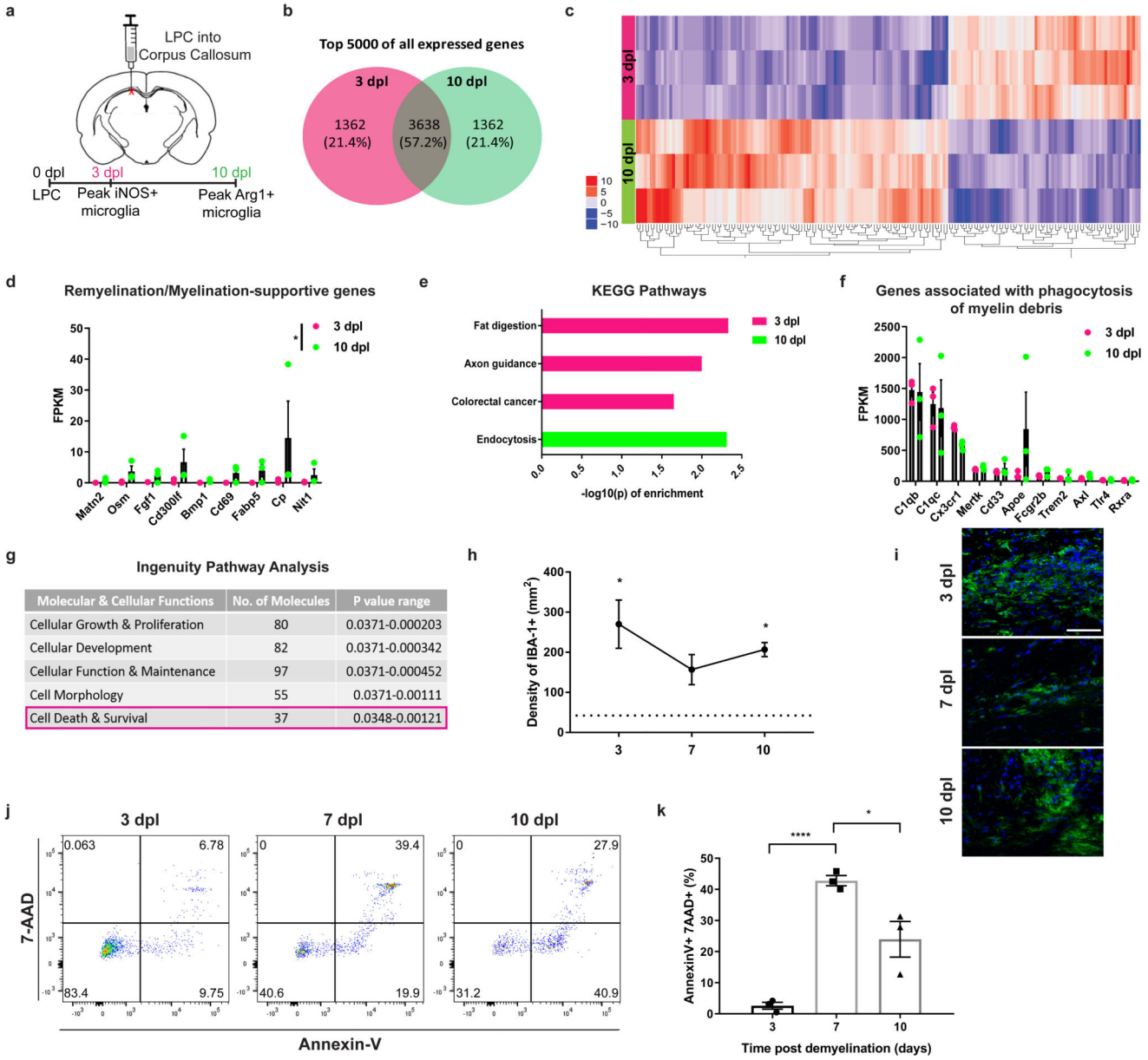

Molecular & Cellular Functions	No. of Molecules	P value range
Cellular Growth & Proliferation	80	0.0371-0.000203
Cellular Development	82	0.0371-0.000342
Cellular Function & Maintenance	97	0.0371-0.000452
Cell Morphology	55	0.0371-0.00111
Cell Death & Survival	37	0.0348-0.00121

Fig. 1. Microglia death occurs during transition in activation following *in vivo* demyelination.

a. Microglia were isolated from focal LPC-demyelinated lesions of mouse corpus callosum, at 3 and 10 dpl representative of key time points of microglial activation during remyelination, for subsequent RNA sequencing.

b. Overlap of top 5000 genes expressed by microglia (including non-significantly differentially expressed) at 3 and 10 dpl, ranked by average Fragments Per Kilobase of transcript per Million (FPKM).

c. Heat map of gene expression level per sample relative to average expression across all samples. Red represents higher expression and blue represents lower expression.

d. Genes with a significant Log_2 fold change ($p<0.05$) in 10 dpl vs 3 dpl microglia with known roles in regulating remyelination, myelination, and the oligodendrocyte lineage,

Europe PMC Funders Author Manuscripts

represented as mean FPKM (± s.e.m.). *P=0.0174 (2-tailed paired Student's *t*-test, t=2.988, df=9). N=3 mice per time point.

e. Kyoto Encyclopedia of Genes and Genomes (KEGG) pathways engaged in genes significantly differentially expressed (p<0.01) by microglia at 3 vs 10 dpl. KEGG pathways are represented on the Y axis and enrichment score on the X axis represented as $-Log_{10}(p)$ enrichment (p<0.05, right-tailed Fisher's Exact Test performed for upregulated and downregulated genes separately).

f. Expression of genes associated with phagocytosis of myelin debris in microglia at 3 and 10 dpl, indicated as mean FPKM (± s.e.m.). No significance between time points, 2-tailed paired *t*-test (P=0.0690, t=2.037, df=10). N=3 mice per time point.

g. Ingenuity Pathway Analysis of significantly engaged molecular and cellular functions in microglia (p<0.05, right-tailed Fisher's Exact Test), indicating 'Cell Death & Survival' as a key pathway.

h. Mean density of IBA-1+ cells per mm^2 (± s.e.m.) of lesioned corpus callosum at 3, 7, and 10 dpl. *P=0.0486 for 3dpl (t=4.371, df=2), P=0.0899 for 7 dpl (t=4.371, df=2), *P=0.011 for 10 dpl (t=4.371, df=2) (2-tailed one sampled *t*-test compared to average density in sham-injected mice; indicated by the dotted line). N=3 mice/ time point.

i. Representative images of lesions in the corpus callosum stained for IBA-1 (green) and counterstained with Hoechst (blue). Scale bar, 50 μm. The experiment performed with 3 mice per time point.

j. Flow cytometry plots of lesion-isolated microglia (CD11b-PeCy7^{+} CD45-BV605^{lo}) positive for cell death markers Annexin-V-FITC and 7-AAD at 3, 7, and 10 dpl. The experiment was performed with 3 mice per time point.

k. Mean proportion of all microglia which are Annexin-V+ 7-AAD+ at 3, 7 and 10 dpl ± s.e.m. ****P<0.0001 3dpl vs 7 dpl (t=20.21, df=4), *P=0.0233 7 dpl vs 10 dpl (t=3.161, df=4). 2-tailed unpaired Student's *t*-test. N=3 mice/time point.

Europe PMC Funders Author Manuscripts

Europe PMC Funders Author Manuscripts

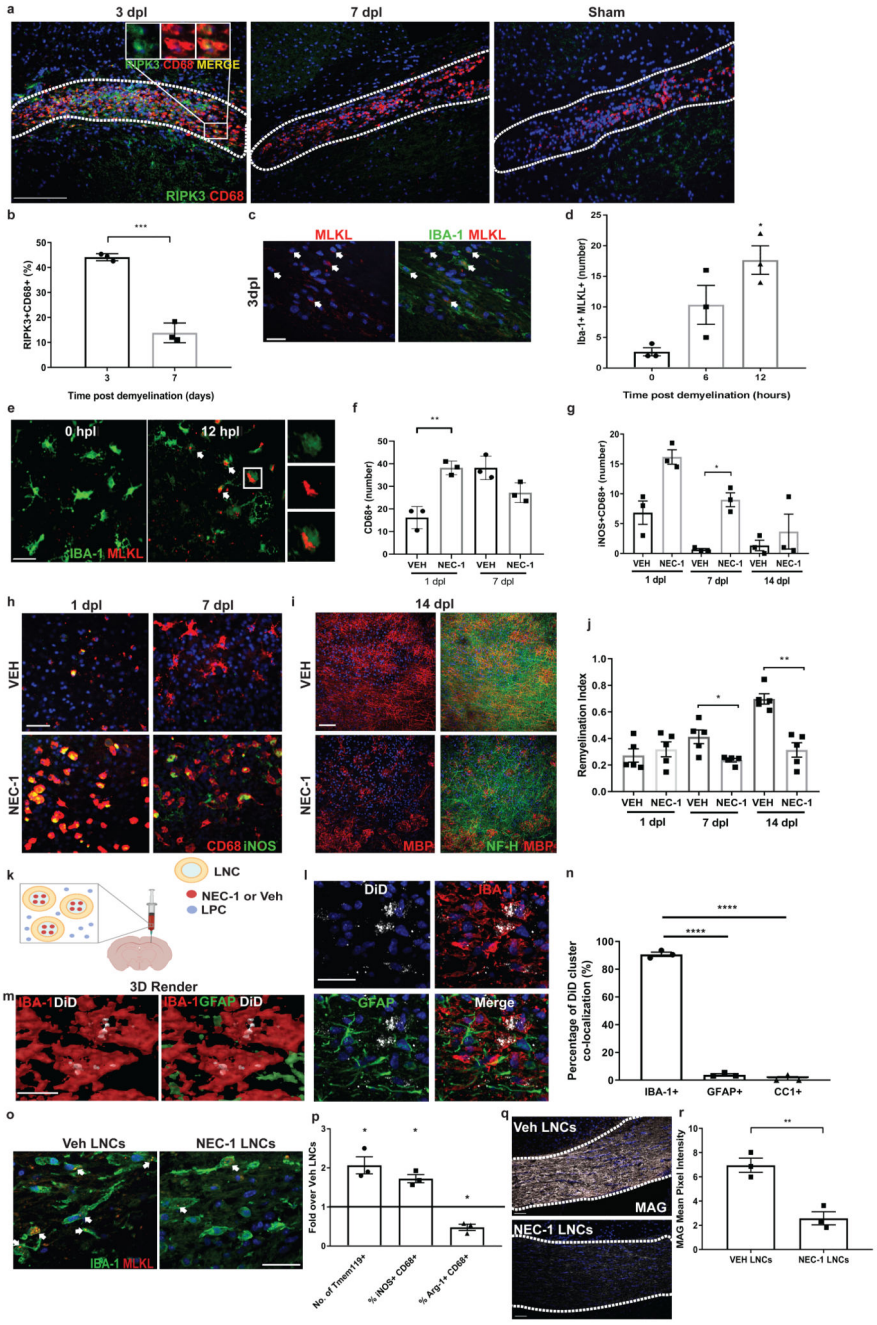

Fig. 2. Pro-inflammatory microglia undergo necroptosis prior to onset of remyelination.

a. *In vivo* lesioned corpus callosum (dotted outline) at 3 and 7 dpl, and sham injection control stained for RIPK3 (green) and CD68 (red). Inset at 3 dpl shows RIPK3+ CD68+ cell. Scale bar, 50μm. The experiment was performed with 3 mice per time point.

b. Mean percentage of RIPK3+ CD68+ microglia / total CD68+ microglia at 3 and 7 dpl in *in vivo* lesioned corpus callosum ± s.e.m.. ***P=0.0002 (2-tailed unpaired Student's *t*-test, t=12.54, df=4). N=3 mice per time point.

c. Images of *in vivo* corpus callosum lesion stained for MLKL (red) and IBA-1 (green) at 3 dpl. Arrows indicate MLKL+ IBA-1+ cells. Scale bar, 10μm. The experiment was performed with 3 mice per time point.

d. Mean number of MLKL+ microglia (IBA-1+) at 0, 6 and 12 hpl in explants ± s.e.m.. *P=0.0219 12 hpl vs 0 hpl (Kruskal-Wallis test, Dunn's Multiple Comparison post-test). N=3 litters.

e. Untreated (0 hpl) and LPC-treated explants (12 hpl) immunostained for IBA-1 (green) and MLKL (red), double positive cells indicated (arrows). Magnified example of a selected IBA-1+ MLKL+ cell (box; right) at 12 hpl. Scale bar, 10 μm. The experiment was performed with 3 litters per time point.

f. Mean number of total microglia (CD68+) at 1 and 7 dpl in NEC-1- or VEH-treated explants ± s.e.m.. **P=0.0027 (2-tailed unpaired Student's *t*-test, t=12.54, df=4). N=3 litters per time point and condition. Quantification derived from images taken at magnification 20X.

g. Mean number of iNOS+ microglia (CD68+) at 1, 7, and 14 dpl in NEC-1- or VEH-treated explants ± s.e.m.. *P=0.05 vs VEH (2-tailed Mann-Whitney test). N=3 litters per time point and condition.

h. Demyelinated explants treated with vehicle (VEH; left) or necrostatin-1 (NEC-1; right) at 1 and 7 dpl immunostained for CD68 (red) and iNOS (green). Scale bar, 20 μm. The experiment was performed with 3 litters per time point.

i. Demyelinated explants treated with VEH (left) or NEC-1 (right) at 14 dpl immunostained for myelin (MBP; red) and axons (NF-H; green). Scale bar, 20 μm. The experiment was performed with 5 litters per time point and condition.

j. Remyelination index of VEH- and NEC-1-treated explants at 1, 7 and 14 dpl ± s.e.m.. *P=0.0159, **P=0.0079 vs VEH (2-tailed Mann-Whitney test). N=5 litters per time point and condition.

k. *In vivo* microglia-targeting of necrostatin (NEC-1) or vehicle control (Veh) using encapsulation in lipidic nanocapsules (LNC), co-injected with LPC into the corpus callosum.

l. Uptake of LNCs labelled with DiD (white) primarily by IBA-1+ cells (red) in lesioned corpus callosum *in vivo*, astrocytes (GFAP+) labelled in green. Scale bar, 20 μm. The experiment was performed with 3 mice per time point.

m. 3D rendering of DiD-LNCs (white) internalized within IBA-1+ cells (red), astrocytes (GFAP+) labelled in green. The experiment was performed with 3 mice per time point. Scale bar, 10 μm.

n. Mean percentage of DiD+ clusters (DiD-LNCs) in lesioned corpus callosum *in vivo* ± s.e.m. co-localized with microglia (IBA-1+), astrocytes (GFAP+) (****P<0.0001, t=21.07, df=4) or oligodendrocytes (CC1+) (****P<0.0001, t=37.26, df=4) (). 2-tailed Student's *t*-test. N=3 mice.

o. Images of *in vivo* lesions at 3 dpl subsequent to treatment with Veh LNCs or NEC-1 LNCs, stained for IBA-1 (green) and MLKL (red). Scale bar, 20 μm. The experiment was performed with 3 mice per time point.

p. Quantification of the mean number of Tmem119+ cells (± s.e.m.) and mean percentage of iNOS+CD68+ (± s.e.m.) or Arg-1+CD68+ (± s.e.m.) (of total CD68+) in 10 dpl *in vivo* lesions subsequent to treatment with NEC-1 LNCs, represented as fold change over values in Veh LNC. *P=0.0395 for Tmem119+ cells (t=4.880, df=2), *P=0.026 for percentage of

iNOS+CD68+ cells (t=6.854, df=2), and *P=0.0224 for percentage of Arg-1+CD68+ cells (t=6.573, df=2) (2-tailed One sample *t*-test compared to a hypothetical value of 1). N=3 mice per stain.

q. Images of *in vivo* corpus callosum at 10 dpl (dotted outline) subsequent to treatment with Veh LNCs or NEC-1 LNCs stained for myelin protein MAG (white). Scale bar, 20 μm. The experiment was performed with 3 mice per time point.

r. Mean MAG pixel intensity in *in vivo* lesions (with respective background intensity outside the lesion subtracted) at 10 dpl following injection with Veh LNCs or NEC-1 LNCs. **P=0.0055 (2-tailed unpaired Student's *t*-test, t=5.465, df=4). N=3 mice per condition.

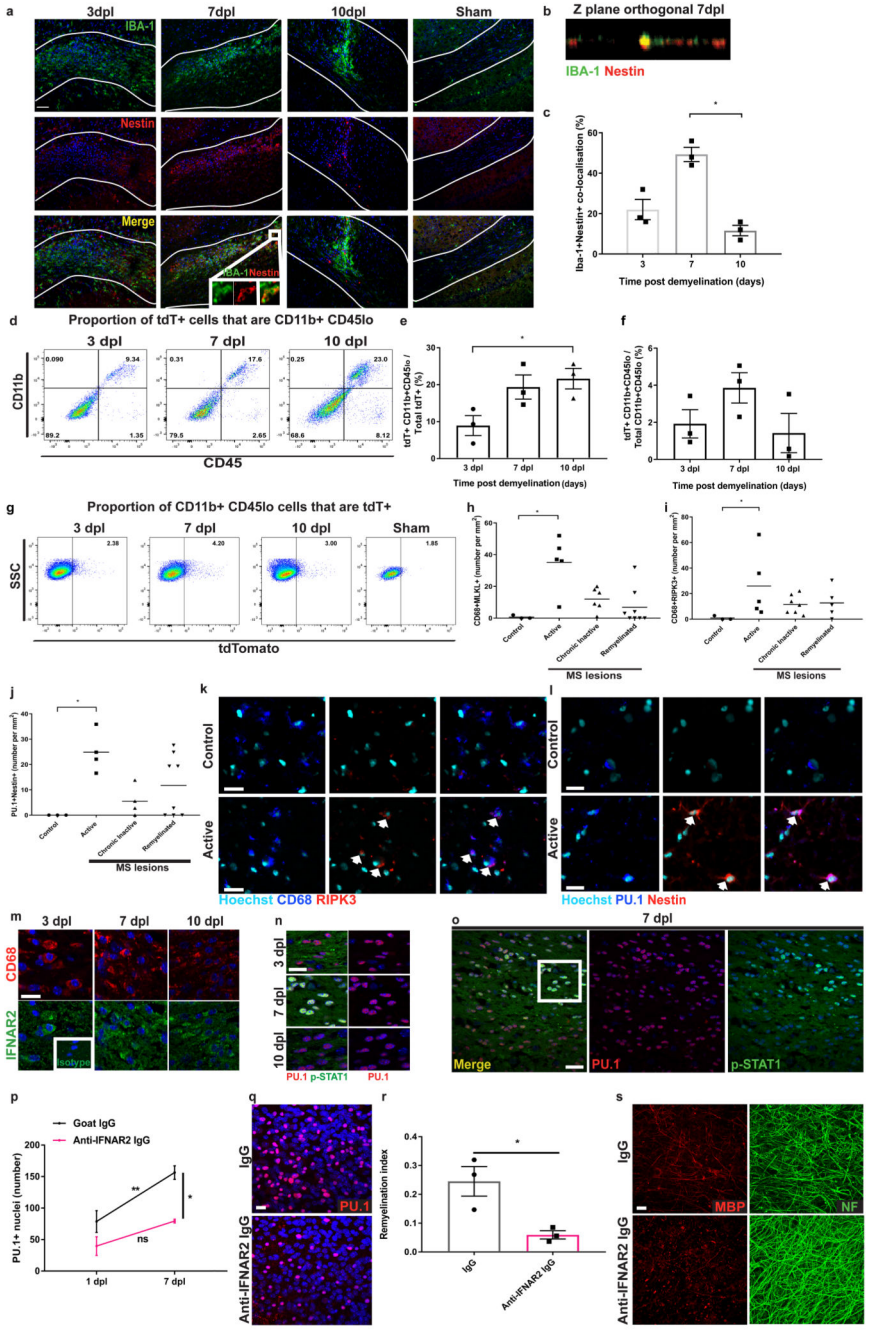

Fig. 3. Microglia repopulation is associated with remyelination in mouse and human white matter and depends on Type-1 interferon signalling.

a. *In vivo* lesions of the corpus callosum (dotted line) at 3, 7 and 10 days post-LPC (dpl), along with sham PBS control (7 days post-surgery) stained for IBA-1 (green) and Nestin (red) Scale bar, 50μM. Inset at 7 dpl demonstrates zoom-in of co-localization of stains. The experiment was performed with 3 mice per time point or condition.

b. Z-plane orthogonal view of 7 dpl *in vivo* lesioned corpus callosum stained for Nestin (red) and IBA-1 (green) demonstrates co-expression. The experiment was performed with 3 mice at 7 dpl.

c. Mean percentage co-localization between IBA-1 and Nestin *in vivo* staining normalized to total IBA-1 signal ± s.e.m.. *P=0.0219 7 dpl vs 10 dpl (Kruskal-Wallis test, Dunn's Multiple Comparison post-test). N=3 mice per time point.

d. Example plot of flow cytometric analysis of proportion of tdTomato+ cells within *in vivo* lesions which are $CD11b^{+}$ $CD45^{lo}$ at 3, 7, and 10 dpl. The experiment was performed with 3 mice per time point.

e. Average percentage of tdTomato (TdT)+ cells ± s.e.m. which are $CD11b^{+}$ $CD45^{lo}$ at 3, 7, and 10 dpl *in vivo*. *P=0.0496 (One-way ANOVA with Tukey's post-hoc test, f=5.376, df=6). N=3 mice per time point.

f. Average percentage of $CD11b^{+}$ $CD45^{lo}$ cells ± s.e.m. which are tdTomato+ at 3, 7, and 10 dpl *in vivo*. N=3 mice per time point.

g. Example plot of flow cytometric analysis of proportion of $CD11b^{+}$ $CD45^{lo}$ cells which are tdTomato+ within *in vivo* lesions at 3, 7, and 10 dpl, compared to sham PBS control. The experiment was performed with 3 mice per time point or condition.

h. Mean density of MLKL+ microglia (CD68+) per mm^2 in control, active, chronic inactive and remyelinated MS lesions. Individual data points represent separate lesions (see Supplementary Table 3). *P=0.0226 active lesions vs control (2-tailed Mann-Whitney test). N=3 control tissues, 5 active lesions, 6 chronic inactive lesions, and 8 remyelinated lesions.

i. Mean density of RIPK3+ microglia (CD68+) per mm^2 in control, active, chronic inactive and remyelinated MS lesions. Individual data points represent separate lesions (see Supplementary Table 1). *P=0.0357 active lesions vs control (2-tailed Mann-Whitney test). N=3 control tissues, 5 active lesions, 6 chronic inactive lesions, and 5 remyelinated lesions.

j. Mean density of Nestin+ PU.1+ cells per mm^2 in control, active, chronic inactive and remyelinated lesions. Individual data points represent separate lesions (see Supplementary Table 3). *P=0.0286 active lesions vs control (2-tailed Mann-Whitney test). N=3 control tissues, 4 active lesions, 4 chronic inactive lesions, and 8 remyelinated lesions.

k. Control brain tissue and active MS lesion immunostained for CD68 (blue) and RIPK3 (red), counterstained with Hoechst (turquoise). Arrows indicate CD68+ RIPK3+ cells. Scale bar, 20 μm. The experiment was performed on 5 active lesions and 3 control tissues.

l. Control brain tissue and active MS lesion immunostained for PU.1 (blue) and Nestin (red), counterstained with Hoechst (turquoise). Arrows indicate PU.1+ Nestin+ cells. Scale bar, 20 μm. The experiment was performed on 4 active lesions and 3 control tissues.

m. *In vivo* remyelinating lesions at 3, 7, and 10 dpl immunostained for CD68 (red) and IFNAR2 (green), counterstained with Hoechst (blue). Inset, rabbit primary isotype control. Scale bar, 10 μm. The experiment was performed on 3 mice per time point.

n. *In vivo* remyelinating lesions at 3, 7, and 10 dpl immunostained for PU.1 (red) and phospho-STAT1 (green), counterstained with Hoechst (blue). Scale bar, 25 μm. The experiment was performed on 3 mice per time point.

o. Representative image of focal *in vivo* lesion at 7 dpl immunostained for PU.1 (red) and phospho-STAT1 (green), counterstained with Hoechst (blue). White square corresponds to panel **n**. Scale bar, 25 μm. The experiment was performed on 3 mice per time point.

Europe PMC Funders Author Manuscripts

p. Mean number of microglia (PU.1+) per field ± s.e.m. in explants at 1 and 7 dpl, treated with anti-IFNAR2 neutralizing antibody or IgG control. **P=0.0098 Goat IgG 1dpl vs 7 dpl (t=4.346, df=8); *P=0.0103 Goat IgG 7 dpl vs anti-IFNAR2 IgG 7 dpl (t=4.309, df=8); P=0.21 anti-IFNAR2 IgG 1 dpl vs anti-IFNAR2 IgG 7 dpl (t=2.220, df=8). One-way ANOVA and Sidak's multiple comparison test, N=3 mice per time point.

q. Explants at 7 dpl treated with anti-IFNAR2 IgG or control IgG, immunostained for PU.1 (red) and counterstained with Hoechst (blue). Scale bar, 10 μm. The experiment was performed with 3 mice per condition.

r. Mean remyelination index of explants at 7 dpl ± s.e.m. treated with anti-IFNAR2 IgG or control goat IgG. *P=0.0252, 2-tailed Student's *t*-test (t=3.485, df=4). N=3 mice per condition.

s. Explants at 7 dpl treated with anti-IFNAR2 IgG or control Goat IgG, immunostained for myelin basic protein (MBP; red) and neurofilament-H (NF; green), showing healthy early remyelination in control and debris in anti-IFNAR2 IgG treatment. Scale bar, 10 μm. The experiment was performed with 3 mice per condition.